ACS APPLIED MATERIALS & INTERFACES

Research Article

www.acsami.org

Solution-Processed Bulk-Heterojunction Solar Cells containing Self-Organized Disk-Shaped Donors

Keisuke Takemoto, Masayoshi Karasawa, and Mutsumi Kimura*

Faculty of Textile Science and Technology, Shinshu University, Ueda 386-8567, Japan

Supporting Information

ABSTRACT: Two molecular disks **1** and **2** composed of a central pyrene core, four oligothiopenes, and peripheral alkyl chains were synthesized and characterized with respect to optical and redox properties in solution and in solid films. It was found that the lowest unoccupied molecular orbital (LUMO) energy levels of **1** and **2** were ideal for achieving efficient electron transfer to fullerene derivatives $PC_{60}BM$ and $PC_{70}BM$, and that **1** and **2** can function as electron donor components in solution-processed bulk-heterojunction (BHJ) solar cells. Disk-shaped molecules **1** and **2** organized ordered structures through intermolecular $\pi-\pi$ interactions as monitored by temperature-controlled polarized optical microscope (TPOM), differential scanning calorimetry (DSC), and powder X-ray diffraction (XRD). Solution-processed BHJ solar cells using **1** or **2** as electron donor materials and fullerene derivatives as acceptor materials were fabricated and investigated. The oligothiophene lengths were reflected in the performance characteristics of solar cell devices fabricated using disk-shaped donors **1** and **2**. Power conversion efficiency (PCE) of 2.6% was achieved for small-molecule BHJ solar cells containing self-organized crystals of **2** in the active layer under one sun condition.

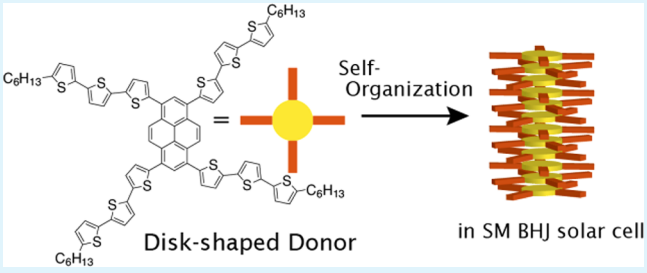

KEYWORDS: *bulk-heterojunction solar cells, pyrene, oligothiophene, stacking, self-organization*

INTRODUCTION

Organic photovoltaic devices have been intensely investigated as a promising candidate for achieving low-cost, flexible, and scalable solar cells. Among the organic photovoltaic devices, power conversion efficiency (PCE) of solution-processed bulk heterojunction (BHJ) solar cells has been rapidly increased through the precise molecular tuning of organic semiconductors, the control of nanostructures within the active layers, and the optimization of device structures.[1,2] To date, PCE has reached 8% for state-of-the-art BHJ solar cells based on conjugated polymer/fullerene blends as reported in scientific literature.[3] Despite the high PCE levels that have been obtained, the device performance of polymer-based BHJ solar cells is stringly affected by the polydispersity of molecular weights and the contamination of trace impurities in the conjugated polymers. To avoid this drawback, discrete and well-defined molecular donors have been designed and applied as the molecular components of active layers in small-molecule BHJ (SM BHJ) solar cells.[4−9] Sun et al. reported on a high conversion efficiency (PCE = 6.7%) for SM BHJ solar cells by using the low-band gap organic donor $DTS(PTTh_2)_2$ and [6,6]-phenyl C_{70}-buthyric acid methyl ester ($PC_{70}BM$).[10] They also found that the addition of solvent additives resulted in the enhancement of PCE due to the reduction of domain sizes in the active layer of SM BHJ solar cells. The control of bicontinuous network structure in the active layers allows a high interfacial area to optimize the exciton dissociation and the efficient transport of the generated charges to the electrodes.[11]

Further improvement in device performance requires the enhancement of charge mobility in the phase-segregated active layers. π-Conjugated disk-shaped molecules such as pyrene, triphenylene, and hexa-*peri*-hexabenzocoronene are attractive molecular units for forming highly ordered one-dimensional stacks through intermolecular $\pi-\pi$ interaction.[12] The large $\pi-\pi$ overlap within self-organized stacks of disk-shaped molecules provides a transport pathway for charge or energy. A three-dimensionally ordered helical liquid crystalline phase of hexahexylthiotriphenylene exhibited a high mobility for photo-induced charge carriers of the order of 0.1 $cm^2\ V^{-1}\ s^{-1}$,[13] and this mobility in the liquid crystalline phase is comparable to that in organic single crystals.[14] High charge mobility of the stacks would be effective for enhancing BHJ solar cell performance.[15−17] Wong et al. reported that hexa-*peri*-hexabenzocorones functionalized with a series of thiophene dendrons exhibited good PCE in SM BHJ solar cells.[15] Lee et al. successfully enhanced PCE in SM BHJ solar cells by using π-stacking of pyrenes in organic donors.[16] In this study, a disk-shaped pyrene with linear oligothiophenes attached to its periphery was investigated as a self-organizing electron donor component in combination with fullerene derivatives in SM BHJ solar cells.

Received: September 6, 2012
Accepted: October 16, 2012
Published: October 16, 2012

Scheme 1. Syntheses of 1 and 2

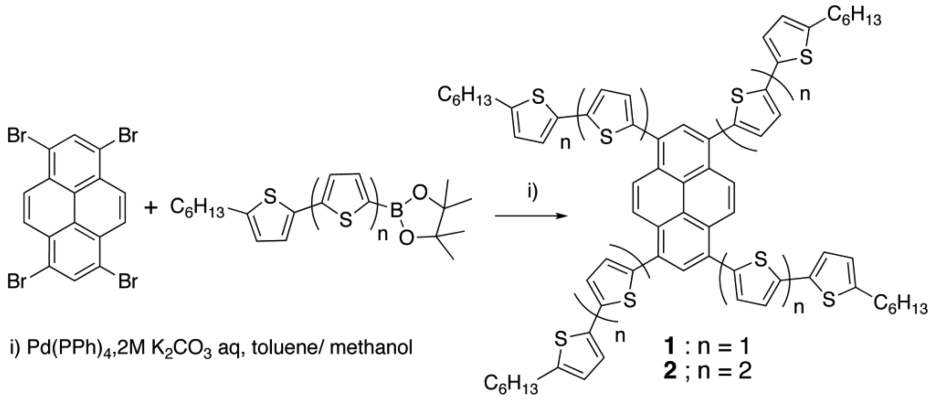

Well-defined oligothiophenes have been synthesized as donor components for SM BHJ solar cells.[18−20] While these oligothiophenes functioned as donor components in SM BHJ solar cells, the cells displayed low PCE values due to their narrow absorption range and poor phase separation. In this study, synthesized X-shaped oligothiophenes **1** and **2** bearing a planar pyrene core were organized into ordered structures in the solid phase and PCE of 2.6% was achieved for a device containing a disk-shaped donor **2** with $PC_{70}BM$ as the acceptor material.

RESULTS AND DISCUSSION

Synthesis of Molecular Disks. We designed two molecular disks **1** and **2**, in which four oligothiophenes were attached at the 1, 3, 6, and 8 positions of a pyrene core (Scheme 1). Disks **1** and **2**, having oligothiophenes of different lengths, were synthesized by the Suzuki-Miyaura coupling reaction between 1, 3, 6, 8-tetrabromopyrene and boronate ester-terminated oligothiophenes in the presence of a palladium catalyst. Purification of **1** and **2** was accomplished by column chromatography followed by recycling preparative HPLC and were unambiguously characterized by means of matrix-assisted laser desorption/ionization time-of-flight mass spectra (MALDI-TOF-MS), analytical HPLC, and ^{1}H and ^{13}C NMR. Analysis of **1** and **2** by MALDI-TOF-MS and HPLC showed no signs of products with defects and confirmed that the coupling of the four oligothiophenes with the focal pyrene core was complete. The peripheral alkyl chains in **1** and **2** provide good solubility in organic solvents such as $CHCl_3$, toluene, n-hexane, and chlorobenzene, and the solubility in $CHCl_3$ is above 0.1 g/mL at 20 °C. Furthermore, the spin-coating process on the glass and quartz substrates resulted in good film forming properties for the synthesized compounds. Good solubility and film forming properties are essential in the fabrication of devices using solution processes.

Optical and Electrochemical Properties. Figure 1 shows absorption and fluorescence spectra of **1** and **2** in $CHCl_3$ (ca. 10^{-5} M), and absorption maxima (λ_{max}), absorption extinction coefficients (ε), and emission maxima (λ_{em}) are listed in Table 1. The positions of absorption and fluorescence peaks shifted to longer wavelengths with increased oligothiophene length, suggesting the formation of a larger π-conjugation system through the pyrene core.[21] Moreover, **2** displayed almost double ε values compared with **1**. The wide absorption range and high ε values of **2** is anticipated to efficient capturing of photon in solar cell devices.

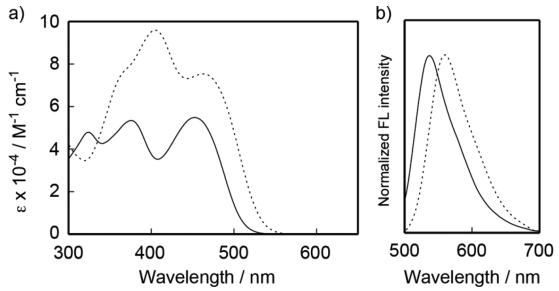

Figure 1. (a) Absorption and (b) fluorescence spectra of **1** (solid line) and **2** (dotted line) in $CHCl_3$.

Table 1. Absorption, Fluorescence, and Electrochemical Data for 1 and 2 in $CHCl_3$ and Solid Film

	solution		film		
compd	λ_{max} (nm) ($\varepsilon \times 10^{-4}$ (M^{-1} cm^{-1}))[a]	λ_{em} (nm)[b]	λ_{max} (nm)[c]	λ_{em} (nm)[c]	$E_{1/2}$ (V vs Fc/Fc$^+$)[d]
1	376 (5.24), 453 (5.37)	537	390, 472	537	0.64
2	405 (9.54), 463 (7.41)	560	438, 501	560	0.46

[a]In $CHCl_3$, [b]In degassed $CHCl_3$. [c]Deposited onto quartz substrate by spin-coating technique from $CHCl_3$ solution. [d]Measured in degassed CH_2Cl_2 containing 0.1 M $TBAPF_6$ at 295 K, scan rate = 100 mV/s.

The energy gap between the highest occupied molecular orbital (HOMO) of the donor and the lowest unoccupied molecular orbital (LUMO) of the acceptor correlate with the potential output of the devices. The HOMO/LUMO energy levels and corresponding band gaps of **1** and **2** were determined by cyclic voltammetry in combination with differential pulse voltammetry in CH_2Cl_2 solution. To determine the first oxidation potentials (E_{ox}) of **1** and **2** in solutions, cyclic voltammetry measurements were performed in CH_2Cl_2 containing 0.1 M tetrabutylammonium hexafluorophosphate ($TBAPF_6$) as a supporting electrolyte. The cyclic voltammograms of **1** and **2** reveal a reversible one-electron oxidation at 0.64 and 0.46 V vs ferrocene/ferricenium redox couple (Fc/Fc$^+$), respectively (Table 1). The observed oxidations of **1** and **2** are attributable to the oxidation of oligothiophene units.[21] The HOMO energy levels of **1** and **2** were estimated to be −5.21 and −5.07 eV from the onset oxidation potential values calibrated by the Fc/Fc$^+$ redox potential vs vacuum. The LUMO energy levels for **1** and **2**, estimated from the HOMO energy levels and the onset of the optical energy gap (E_{0-0}), are

evaluated to be −2.73 and −2.71 eV. The HOMO energy level of **2** is higher than that of **1**, whereas the LUMO energy level of **2** is almost the same as that of **1**. The LUMO energy levels of **1** and **2** are higher than those of $PC_{60}BM$ and $PC_{70}BM$, revealing sufficient driving force for efficient charge separation after photoexcitation. The disk-shaped molecules **1** and **2** having oligothiophenes are expected to be a suitable candidate for electron donor components in BHJ solar cells with $PC_{60}BM$ or $PC_{70}BM$.

Self-Organizing Properties. Pyrene-containing molecules can organize into highly anisotropic and ordered structures through intermolecular $\pi-\pi$ stacking.[22−24] The self-organizing materials tend to eliminate structural and electronic defects by self-healing, and their fluidity allows for easy preparation of thin films. The absorption and fluorescence spectra of thin films were broadened and red-shifted compared to those in solution (Table 1). These spectral changes can be ascribed to the formation of molecular aggregates in the thin film.[25,26]

The thermotropic behaviors of **1** and **2** have been investigated by means of differential scanning calorimetry (DSC), thermogravimetric analysis (TGA), and temperature-controlled polarizing optical microscopy (TPOM). Additional characterization of the organized structures was performed by powder X-ray diffraction (XRD). The DSC traces of **1** and **2** showed one endothermic peak at 155 and 172 °C. The XRD patterns of **1** and **2** displayed many deflections in the wide-angle region, and no mesomorphic behavior was observed in TPOM studies. Weight losses in the TGA analysis of **1** and **2** started at 304 °C. On the basis of these results, we attribute the transition in the DSC measurements to the melting point. When **1** and **2** are slowly cooled down from the melting points, they form large crystalline domains as shown in Figure 2a. The XRD pattern of **2** in the short-angle region at 170 °C gave three Bragg reflections in the ratio $1:1/\sqrt{3}:1/2$, indicating that the organized phase consists of a two-dimensional hexagonal lattice with a lattice constant a = 3.27 nm (Figure 2b). The lattice constant is fairly close to that of the rigid segment (2.8 nm) within **2** as estimated from the molecular model. The XRD pattern of **1** also showed a hexagonal lattice with a = 2.90 nm. In addition, **2** exhibited two intense reflections at 0.42 and 0.48 nm in the wide-angle region. The distance of 0.48 nm is consistent with the stacking distance among pyrene units of the liquid-crystalline hexagonal columnar phase of pyrene-based molecules reported by Hayer et al.[27] The absorption spectrum of the thin film of **2** after annealing at 150 °C showed a new shoulder peak at 560 nm, which is indicative of intermolecular aggregation of the oligothiophene units in **2** (Figure 2c).[25,26] In contrast, the spectrum of the thin film of **1** remained unaltered after the annealing. From these results, we concluded that the pyrene-cored compounds **1** and **2** having oligothiophene units can organize into ordered structures through π-orbital associations in the solid state.

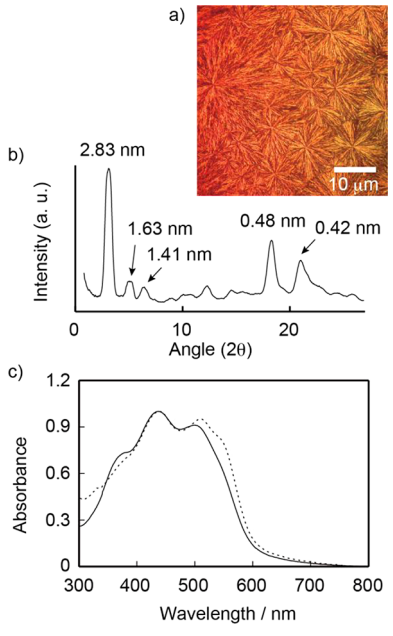

Figure 2. (a) Polarized optical micrograph of **2** at 170 °C after cooling form the isotropic phase. (B) Temperature-controlled XRD pattern of **2** at 170 °C. (c) Absorption spectra of a thin film of **2** before (solid line) and after annealing at 150 °C for 10 min (dotted line).

Device Performance of SM BHJ Solar Cells. The active layers in the BHJ solar cells compose the interpenetrating bicontinuous network structures of an electron donating molecules and an electron accepting fullerene derivatives.[1,2] Control of the phase-segregation structure in the blended active layers is an important factor in enhancing the PCE of BHJ solar cells. The surface morphology of blended films was examined by tapping mode atomic force microscopy (AFM). The topographic and phase AFM images of a thin blended film composed of **2** and $PC_{70}BM$ (**2**:$PC_{70}BM$ = 1:4 w/w) are shown in Figure 3. The samples were prepared by spin coating of

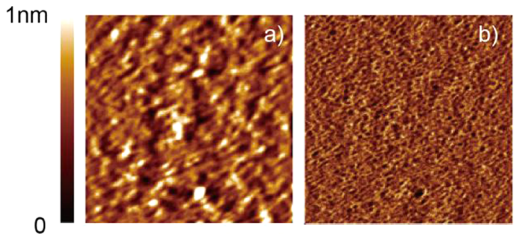

Figure 3. Tapping-mode AFM (a) height and (b) phase images (500 × 500 nm^2) of **2**/$PC_{70}BM$ blended film in a weight ratio of 1:4.

$CHCl_3$ solution of **2** and $PC_{70}BM$ on a glass substrate and the resulting thin films were annealed at 150 °C for 10 min under an Ar atmosphere. The surface morphology of the annealed film is very smooth with an average surface roughness of 1.2 nm. Phase images provide information about donor and acceptor distribution in active layers.[28] The phase image in Figure 3b reveals the presence of two domains having different material stiffness. The two domains can be assigned to the acceptor-rich domain and donor-rich domain. The AFM image indicates that **2** has a good miscibility with $PC_{70}BM$ in the blended films, and that the spontaneous phase-segregation process in the mixed layer can form a bicontinuous network structure, which acts as percolation channels for the efficient carrier collection within the active layer of BHJ solar cells. The XRD pattern of blended films stayed unchanged as compared with those of **2**, and additional broad diffractions corresponding to neat C_{60} samples appeared around 0.8 nm.[29] Pyrene-cored compounds retain ordered structures within the phase-segregated films. The blending with fullerene derivatives does not affect the ordered structures in the donor domains composed of **1** or **2**, and phase segregation between the

Table 2. Summary of device parameters of SM BHJ solar cells based on mixed active layers composed of self-organized disk-shaped donors 1 and 2 and PCBMs with different composition ratios

active layer (weight ratio)	thickness (nm)	J_{sc} (mA cm^{-2})	V_{oc}(mV)	FF	PCE (%)	IPCE$_{max}$ (%)
1/$PC_{60}BM$ (1:4)	50	3.2	760	0.30	0.7	43
1/$PC_{60}BM$ (1:5)	50	3.8	880	0.35	1.2	50
1/$PC_{60}BM$ (1:6)	50	3.3	780	0.32	0.8	48
2/$PC_{60}BM$ (1:3)	50	4.0	780	0.36	1.1	43
2/$PC_{60}BM$ (1:4)	50	5.7	800	0.38	1.7[a]	65
2/$PC_{60}BM$ (1:5)	50	4.0	820	0.36	1.2	43
1/$PC_{70}BM$ (1:5)	50	6.9	910	0.36	2.2	62
2/$PC_{70}BM$ (1:4)	50	8.8	830	0.36	2.6	84
P3HT/$PC_{60}BM$ (2:1)	70	7.5	610	0.61	2.8	67

[a]The PCE of SM BHJ solar cell without the thermal annealing was 0.2%.

organic donors and the fullerene derivatives has occurred in the thin films.

SM BHJ solar cells were fabricated using **1** and **2** as the electron donor materials and fullerene derivatives as the electron acceptor materials through the conventional spin-coating process. The cleaned tin-doped indium oxide (ITO)-coated glass anode was modified by spin-coating on poly(3,4-ethylenedioxythiophene):polystylenesulfonate (PEDOT:PSS) as a hole-extraction/electron-blocking layer with 40 nm thickness. The active layer was deposited from the mixed $CHCl_3$ solutions onto the PEDOT:PSS modified ITO anodes in the argon-filled glovebox ($[O_2]$ < 0.1 ppm and $[H_2O]$ < 0.1 ppm), and the thickness was typically 50 nm. After spin-coating, the resulting active layer was annealed at 150 °C for 10 min. TiO_x on the blended active layer has been used as an electron collection layer in the BHJ solar cells.[30] Finally, aluminum cathode was deposited through a shadow mask by thermal evaporation under vacuum. The effect of different compositions between **2** and $PC_{60}BM$ was investigated and device performance parameters are summarized in Table 2. The device fabricated from the mixed solution with **2**: $PC_{60}BM$ composition of 1: 3 w/w showed a PCE of 1.1%, with a short-circuit current (J_{sc}) of 4.0 mA cm^{-2}, an open circuit voltage (V_{oc}) of 0.78 V and a fill factor of 36%. After increasing the **2**: $PC_{60}BM$ composition ratio to 1: 4, the PCE increased to 1.7%. The device shows a drop in PCE value as the fullerene loading is further increased. Our optimized devices based on **1** and **2** require the high content of n-type fullerenes.

Figure 4a shows the $J-V$ curves of BHJ solar cells fabricated using **1** and **2** with $PC_{60}BM$. The J_{sc} value of the **2**/$PC_{60}BM$ device is higher than that of the **1**/$PC_{60}BM$. The incident-photon to current conversion efficiency (IPCE) spectra followed the absorption feature of oligothiophene-substituted pyrene and $PC_{60}BM$, as shown in Figure 4b. The IPCE values of the **2**/$PC_{60}BM$ device are higher than those of **1**/$PC_{60}BM$ in all visible light regions. The IPCE difference between **1** and **2** is due to the wider absorption spectral range and the higher ε value of **2** relative to **1**. The V_{oc} value of the **2**/$PC_{60}BM$-based device is slightly lower than that of the **1**/$PC_{60}BM$. The V_{oc} of BHJ solar cells depends on the energy gap between the donor HOMO level and the acceptor LUMO level.[31] The energy gaps of 1.1 and 1.0 eV for **1**/$PC_{60}BM$ and **2**/$PC_{60}BM$ agreed with the difference in V_{oc} values for the devices.

Figure 5 shows the $J-V$ and IPCE characteristics of a **2**/$PC_{70}BM$ device (**2**: $PC_{70}BM$ composition ratio =1: 4 w/w). The J_{sc} value was improved significantly by changing from $PC_{60}BM$ to $PC_{70}BM$. The PCE of the **2**/$PC_{70}BM$ device was 2.6% under one sun condition, and the device exhibited a

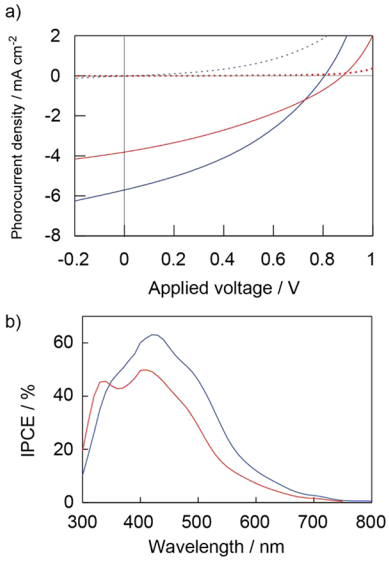

Figure 4. (a) Photocurrent voltage curve obtained with SM BHJ solar cells based on **1**/$PC_{60}BM$ (1:5 w/w, red line) and **2**/$PC_{60}BM$ (1:4 w/w, blue line) blended active layers under a standard global AM 1.5 solar condition (solid line) and dark current (dotted line). (b) Incident photon-to-current conversion efficiency spectrum based on SM BHJ solar cells based on **1**/$PC_{60}BM$ (1:5 w/w, red line) and **2**/$PC_{60}BM$ (1:4 w/w, blue line) blended active layers.

maximum IPCE value of 84% at 480 nm (Table 2). The wider absorption range of $PC_{70}BM$ compared to $PC_{60}BM$ can improve light harvesting in the solar cells. The PCE of the **2**/$PC_{70}BM$ device is slightly lower than that of a poly(3-hexylthiophene) (P3HT)/$PC_{60}BM$ device. While the HOMO level of P3HT (−5.06 eV) is almost the same as that of **2**, the V_{oc} value of the **2**/$PC_{70}BM$ device (V_{oc} = 0.83 V) is higher than that of the P3HT/$PC_{60}BM$ device (V_{oc} = 0.61 V). Several organic donor materials for SM BHJ solar cells also showed higher V_{oc} values than the P3HT/$PC_{60}BM$ device.[4−9] The lower fill factor (FF) value in the **2**/$PC_{70}BM$ device indicates the poor balance of charge carrier mobilities in the phase-segregated active layer. Studies are now in progress to examine the charge mobility of blended films containing self-organized domains made of **2** by a photo-CELIV technique and to elucidate the mechanisms of photoinduced charge transfer by transient absorption studies.

CONCLUSION

In summary, we have presented simple molecular disks functionalized with lengthy oligothiophene units for the

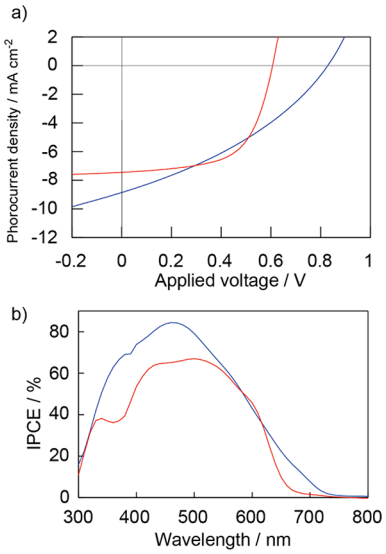

Figure 5. (a) Photocurrent voltage curve obtained with SM BHJ solar cells based on **2**/$PC_{70}BM$ (1:4 w/w, blue line) and P3HT/$PC_{60}BM$ (2:1 w/w, red line) blended active layers under a standard global AM 1.5 solar condition. (b) Incident photon-to-current conversion efficiency spectrum based on SM BHJ solar cells based on **2**/$PC_{70}BM$ (1:4 w/w, blue line) and P3HT/$PC_{60}BM$ (2:1 w/w, red line) blended active layers.

molecular component of SM BHJ solar cells. The optical and electronic properties of molecular disks can be tuned by changing the length of oligothiophenes. Molecular disks possessing peripheral alkyl chains can organize into organized structures through intermolecular $\pi-\pi$ interactions, as we are able to conclude from absorption spectral changes in thin films, DSC, TPOM, and XRD. The pyrene core within the molecular disks was employed as the scaffold for molecular organization. A spontaneous phase-segregation process between molecular disks and fullerene derivatives formed bicontinuous network structures confirmed by AFM measurement. The formation of these structures is favorable for achieving efficient charge transport after photoexcitation. The SM BHJ solar cells fabricated with the molecular disks as electron donor components exhibited a good performance achieving PCE of 2.6%. The high IPCE value above 80% at the absorption maximum of **2** indicated an almost complete conversion of photon at this wavelength into electron. The further molecular designing of molecular disks can enhance the PCE values of solution-processed BHJ solar cells by optimizing the organized structures of donors for efficient charge mobility in the active layers, as well as expanding absorption ranges of organic donors to enhance their light-harvesting properties.

EXPERIMENTAL SECTION

General. NMR spectra were recorded on a Bruker AVANCE 400 FT NMR spectrometer at 399.65 and 100.62 MHz for ^1H and ^{13}C in $CDCl_3$ solution. Chemical shifts are reported relative to internal TMS. IR spectra were obtained on a SHIMAZU IR Prestige-21 with DuraSample IR II. UV−vis spectra were measured on a JASCO V-650. MALDI-TOF mass spectra were obtained on a Bruker autoflex with dithranol as matrix. The optical textures were studies a Nikon polarizing microscope equipped with a Mettler Toledo FP82 hot stage. The transition temperatures were measured by differential scanning calorimetry with a SII DSC 6200 operated at a scanning rate of 10 °C min^{-1} on heating and cooling. The apparatus was calibrated with indium as standard. The XRD patterns were obtained with a Rigaku XRD-DSC with Cu Kα radiation. Atomic force microscopy images were acquired in noncontact mode by a JEOL JSPM-5400 system. The samples for AFM were prepared by the spin-coating of $CHCl_3$ solutions on glass substrate.

Cyclic voltammetric measurements were recorded on an ALS 700 potentiostat using a three cell electrode system with a Pt working electrode, a Pt counter electrode, and an Ag/AgCl reference electrode. $TBAPF_6$ was used as the electrolyte.

Materials. All chemicals were purchased from commercial suppliers and used without purification. P3HT was purchase from Aldrich (electronic grade) and used without any purification. 1,3,6,8-Tetrabromopyrene,[23,32] 5′-hexyl-2,2′-bithiophene-5-boronic acid pinacol ester, and 5″-hexyl-2′,2″:5″,2′-terthiophene-5-boronic acid pinacol ester were synthesized by standard procedures. Column chromatography was performed with silica gel (Wakogel C-200). Recycling preparative gel permeation chromatography was carried out by a JAI recycling preparative HPLC using $CHCl_3$ as an eluent. Analytical thin layer chromatography was performed with commercial Merck plates coated with silica gel 60 F_{254} or aluminum oxide 60 F_{254}. The purities of target compounds were confirmed by NMR, MALDI-TOF-Ms and analytical HPLC (column: Inertsil C18 (GL Science Inc.), eluent: $CHCl_3$, purity was determined by the ratio between the peak area of compound and the total peak area).

1: A solution of 1, 3, 6, 8-tetrabromopyrene (0.1 g, 0.19 mmol), 5′-hexyl-2,2′- bithiophene-5-boronic acid pinacol ester (0.57 g, 1.54 mmol) and $Pd(PPh_3)_4$ (57 mg, 49 μmol) in toluene (12.5 mL), ethanol (4.0 mL) and 2.0 M K_2CO_3 aqueous solution (2.5 mL) was stirred at 120 °C for 48 h under nitrogen. After cooling to room temperature, the reaction mixture was poured into water, extracted with CH_2Cl_2. The organic layer was dried over magnesium sulfate and the solvent was evaporated. The residue was purified by column chromatography on silica gel by eluting with CH_2Cl_2 and recycling preparative HPLC to give **1** as orange solid (0.23 g, yield 84%). ^1H NMR (400.13 MHz, $CDCl_3$): δ (ppm) = 8.58 (s, 4H, Ar*H*), 8.23 (s, 2H, Ar*H*), 7.28 (d, J = 3.6 Hz, 4H, Ar*H*), 7.22 (d, J = 3.6 Hz, 4H, Ar*H*), 7.06 (d, J = 3.6 Hz, 4H, Ar*H*), 6.72 (d, J = 3.6 Hz, 4H, Ar*H*), 2.82 (t, J = 7.6 Hz, 8H, $-CH_2-$), 1.71 (m, 8H, $-CH_2-$), 1.37 (m, 24H, $-CH_2-$), 0.91 (t, J = 6.6 Hz, 12H, $-CH_3$); ^{13}C NMR ($CDCl_3$, 100.61 Hz): δ (ppm) =145.7, 140.0, 139.3, 134.6, 129.6, 129.0, 128.9, 125.7, 124.9, 123.6, 123.5, 31.6, 30.2, 28.8, 22.6, 14.1. MALDI-TOF-Ms: m/z = 1194 (M+H, 100%) calculated for $C_{72}H_{74}S_8$. Anal. Calcd for $C_{72}H_{74}S_8$: C, 72.31; H, 6.24. Found: C, 72.4; H, 6.3. Purity (HPLC) > 99%.

2: Compound **2** was synthesized from 1,3,6,8-tetrabromopyrene and 5″-hexyl-2′,2″:5″,2′-terthiophene-5-boronic acid pinacol ester according to the same procedure of **1**. Yield 73%. ^1H NMR (400.13 MHz, $CDCl_3$): δ (ppm) =8.49(s, 4H, Ar*H*), 8.21(s, 2H, Ar*H*), 7.26(m, 8H, Ar*H*), 7.12(m, 4H, Ar*H*), 7.02(m, 8H, Ar*H*), 6.71(d, J = 3.6 Hz, 4H, Ar*H*), 2.83(t, J = 7.6 Hz, 8H, $-CH_2-$), 1.72(m, 8H, $-CH_2-$), 1.39(m, 24H, $-CH_2-$), 0.93(t, J = 7.2 Hz, 12H, $-CH_3$); ^{13}C NMR ($CDCl_3$, 100.61 Hz): δ (ppm) =145.6, 140.6, 138.5, 137.0, 135.3, 134.5, 129.1, 128.5, 124.8, 124.4, 123.9, 123.6, 123.4, 31.6, 30.2, 28.8, 22.6, 14.1. MALDI-TOF-Ms: m/z = 1522 (M+H, 100%) calculated for $C_{88}H_{82}S_{12}$. Anal. Calcd for $C_{88}H_{88}S_{12}$: C, 69.34; H, 5.42. Found: C, 69.2; H, 5.4. Purity (HPLC) > 99%.

Fabrication of SM BHJ Solar Cells. Indium tin oxide (ITO) patterned glass substrates were cleaning with sonication in neutral detergent, distilled water, acetone and 2-propanol. The substrates were dried and apply UV−O_3 treatment for 30 min. Electron blocking layer were prepared by spin-coated the PEDOT:PSS (H. C. Starck) with a thickness of 40 nm. The substrates were baked at 200 °C for 30 min. A solution containing a mixture of pyrene-cored donors and fullerene derivatives in chloroform were spin-coated onto the PEDOT: PSS layer and apply thermal annealing treatment at 150 °C for 10 min in the argon filled globe box. Titanium oxide solution was spin-coated onto the active layer then place in air for 30 min.[28] The counter electrode of aluminum was prepared by thermal deposition with a thickness of 100 nm. Current density−voltage ($J-V$) characteristics were measured using a Keithley 2400 Source Measure Unit. Performance of BHJ solar cells devices was measured under one-sun

conditions (AM 1.5, 100 mW cm^{-2}) by a solar simulator (XES-151S, Sanei electric Inc.).

■ ASSOCIATED CONTENT

Ⓢ Supporting Information

^{1}H NMR spectra, DSC, XRD, and AFM image. This material is available free of charge via the Internet at http://pubs.acs.org.

■ AUTHOR INFORMATION

Corresponding Author

*E-mail: mkimura@shinshu-u.ac.jp.

Notes

The authors declare no competing financial interest.

■ ACKNOWLEDGMENTS

We acknowledge financial support from the New Energy and Industrial Technology Development Organization (NEDO) of Japan. We thank Prof. Kazuchika Ohta of Shinshu University for valuable discussions on the crystalline structures.

■ REFERENCES

(1) Günes, S.; Neugebauer, H.; Sariciftci, N. S. *Chem. Rev.* **2007**, *107*, 1324−1338.

(2) Thompson, B. C.; Fréchet, J. M. J. *Angew. Chem., Int. Ed.* **2008**, *47*, 58−77.

(3) Dou, L.; You, J.; Yang, J.; Chen, C.-C.; He, Y.; Murase, S.; Moriarty, T.; Emery, K.; Yang, T. *Nat. Photonics* **2012**, *6*, 180−185.

(4) Boudreault, P.-L. T.; Najari, A.; Leclerc, M. *Chem. Mater.* **2011**, *23*, 456−469.

(5) Walker, B.; Kim, C.; Nguyen, T.-Q. *Chem. Mater.* **2011**, *23*, 470−482.

(6) Mishra, A.; Bäuerle, P. *Angew. Chem., Int. Ed.* **2012**, *51*, 2020−2067.

(7) Silvestri, F.; Irwin, M. D.; Beverina, L.; Facchetti, A.; Pagani, G. A.; Marks, T. J. *J. Am. Chem. Soc.* **2008**, *130*, 17640−17641.

(8) Matsuo, Y.; Sato, Y.; Niinomi, T.; Soga, I.; Tanaka, H.; Nakamura, E. *J. Am. Chem. Soc.* **2009**, *131*, 16048−16050.

(9) Walker, B.; Tamayo, A. B.; Dang, X.-D.; Zalar, P.; Seo, J. H.; Tantiwiwat, M.; Nguyen, T. −Q. *Adv. Funct. Mater.* **2009**, *19*, 3063−3069.

(10) Sun, Y.; Welch, G. C.; Leong, W. L.; Takacs, C. J.; Bazan, G. C.; Heeger, A. J. *Nat. Mater.* **2012**, *11*, 44−48.

(11) Ma, W.; Yang, C.; Gong, X.; Lee, K.; Heeger, A. J. *Adv. Funct. Mater.* **2005**, *15*, 1617−1622.

(12) Kaafarani, B. R. *Chem. Mater.* **2011**, *23*, 378−396.

(13) Adam, D.; Schuhmacher, P.; Simmerer, J.; Haussling, L.; Siemensmeyer, K.; Etzbachi, K. H.; Ringsdorf, H.; Haarer, D. *Nature* **1994**, *371*, 141−143.

(14) van de Craats, A. M.; Warman, J. M. *Adv. Mater.* **2001**, *13*, 130−133.

(15) Wong, W. W. H.; Ma, C.-Q.; Pisula, W.; Yan, C.; Feng, X.; Jones, D. J.; Müllen, K.; Janssen, R. A. J.; Bäuerle, P.; Holms, A. B. *Chem. Mater.* **2010**, *22*, 457−466.

(16) Lee, O. P.; Beaujuge, P. M.; Woo, C. H.; Holcombe, T. W.; Millstone, J. E.; Douglas, J. D.; Chen, M. S.; Fréchet, J. M. J. *Adv. Mater.* **2011**, *23*, 5359.

(17) Kang, S. J.; Kim, J. B.; Chiu, C. −Y.; Ahn, S.; Schiros, T.; Lee, S. S.; Yager, K. G.; Toney, M. F.; Loo, Y.-L.; Nuckolls, C. *Angew. Chem., Int. Ed.* **2012**, *51*, 8594−8597.

(18) Ma, C.-Q.; Mena-Osteritz, E.; Debaerdemaeker, T.; Wienk, M. M.; Janssem, R. A. J.; Bäuerle, P. *Angew. Chem., Int. Ed.* **2007**, *46*, 1679−1683.

(19) Ma, C.-Q.; Fonrodona, M.; Schikora, M. C.; Wienk, M. M.; Janssen, R. A. J.; Bäuerle, P. *Adv. Funct. Mater.* **2008**, *18*, 3323−3331.

(20) Liu, Y.; Wan, X.; Wang, F.; Zhou, J.; Long, G.; Tian, J.; You, J.; Yang, Y.; Chen, Y. *Adv. Energy Mater.* **2011**, *1*, 771−775.

(21) Bäuerle, P. *Adv. Mater.* **1992**, *2*, 102−107.

(22) Figueira-Duarte, T. M.; Müllen, K. *Chem. Rev.* **2011**, *111*, 7260−7314.

(23) Uchiyama, M.; Watanabe, Y.; Araoka, F.; Watanabe, J.; Takezoe, H.; Konishi, G. *Adv. Mater.* **2010**, *22*, 4473−4478.

(24) Moorthy, J. N.; Natarajan, P.; Venkatakrishnan, P.; Huang, D.-F.; Chow, T. J. *Org. Lett.* **2007**, *9*, 5215−5218.

(25) Murphy, A. R.; Chang, P. C.; VanDyke, P.; Liu, J.; Fréchet, J. M. J.; Subramanian, V.; DeLongchamp, D. M.; Sambasivan, S.; Fisher, D. A.; Lin, E. K. *Chem. Mater.* **2005**, *17*, 6033−6041.

(26) Samitsu, S.; Shimomura, T.; Heike, S.; Hashizume, T.; Ito, K. *Macromolecules* **2008**, *41*, 8000−8010.

(27) Hayer, A.; de Halleux, V.; Köhler, A.; El-Garoughy, A.; Meijer, E. W.; Barberá, J.; Tant, J.; Levin, J.; Lehmann, M.; Gierschner, J.; Cornil, J.; Geerts, Y. H. *J. Phys. Chem. B* **2006**, *110*, 7653−7659.

(28) Slota, J. E.; He, X.; Huch, W. T. S. *Nano Today* **2010**, *5*, 231−242.

(29) Guo, J.; Liang, Y.; Szarko, J.; Lee, B.; Son., H. J.; Rolczynski, B. S.; Yu, L.; Chen, L. X. *J. Phys. Chem. B* **2010**, *114*, 742−748.

(30) Hayakawa, A.; Yoshiokawa, O.; Fujieda, T.; Uehara, K.; Yoshikawa, S. *Appl. Phys. Lett.* **2007**, *90*, 163517.

(31) Scharber, M. C.; Mühlbacher, D.; Koppe, M.; Denk, P.; Waldauf, C.; Heeger, A. J.; Brabec, C. J. *Adv. Mater.* **2006**, *18*, 789−794.

(32) Stylianou, K. C.; Heck, R.; Chong, S. Y.; Bacsa, J.; Jones, J. T. A.; Khimyak, Y. Z.; Bradshaw, D.; Rosseinsky, M. J. *J. Am. Chem. Soc.* **2010**, *132*, 4119−4130.